

NBSIR 88-3084

# POSSIBLE DESIGNS FOR ELECTRIC-FIELD-STRENGTH PROBES FOR MILLIMETER WAVES

---

---

J. Randa  
M. Kanda  
D. Melquist

National Bureau of Standards  
U.S. Department of Commerce  
Boulder, Colorado 80303-3328

February 1988

QC  
100  
.U56  
#88-3084  
1988  
c.2



NBSIR 88-3084

# POSSIBLE DESIGNS FOR ELECTRIC-FIELD-STRENGTH PROBES FOR MILLIMETER WAVES

---

---

NBS  
D-100  
U.S.  
NO. 88-3084  
1988  
217

J. Randa  
M. Kanda  
D. Melquist

Electromagnetic Fields Division  
Center for Electronics and Electrical Engineering  
National Engineering Laboratory  
National Bureau of Standards  
Boulder, Colorado 80303-3328

February 1988

Sponsored by  
Naval Ocean Systems Center  
San Diego, California 92152-5122



---

U.S. DEPARTMENT OF COMMERCE, C. William Verity, Secretary

NATIONAL BUREAU OF STANDARDS, Ernest Ambler, Director



POSSIBLE DESIGNS FOR ELECTRIC-FIELD-STRENGTH PROBES  
FOR MILLIMETER WAVES

J. Randa, M. Kanda, and D. Melquist  
Electromagnetic Fields Division - 723.03  
National Bureau of Standards  
Boulder, CO 80303

Various designs are considered for electric-field probes for the frequency range 26-110 GHz. Two particular designs are investigated in some detail. A resistively tapered dipole antenna with a diode detector shows promise for frequencies up to about 40 GHz. The second design is based on a fiber-optically sensed temperature sensor to detect the heating of a resistive strip. If its sensitivity can be increased significantly, this design may be capable of operating to frequencies above 100 GHz.

Key words: electric-field probe; flouroptic temperature sensor; millimeter waves; resistively tapered dipole.

## I. INTRODUCTION

With the growing importance of millimeter waves in both military and civilian applications comes an increased demand for electric-field probes to operate at frequencies up to 100 GHz and beyond. Such probes would be useful in many applications, but the one of interest in the present study is as a transfer standard, enabling secondary calibration facilities to trace their measurements back to a primary standards laboratory. Transfer standard probes of this sort which the National Bureau of Standards (NBS) has developed in the past include the EFM-5 [1] and the 8-mm resistively tapered dipole [2]. The frequency ranges for these two electric-field probes extend to 1 GHz and 18 GHz respectively. There are electric-field probes available commercially which are claimed to work to higher frequencies, but they are not suitable for our purposes.

In developing a probe design for electric fields up to 110 GHz, we will pursue three different lines of attack. The most conservative approach is to attempt to extend a successful lower-frequency design into the frequency range of interest. The resistively tapered 8-mm probe, whose highest operating frequency is about 18 GHz, will be the starting point for this attempt. The dipole will be scaled down from 8 mm to 4 or 2 mm, and a diode whose range includes the higher frequencies will be used as a detector. The second approach is to use an antenna other than a short dipole -- a commercially available broadband antenna better suited to the millimeter wave region. We will present estimates of the parameters and performance required for a spiral antenna. Attempts to obtain a suitable antenna commercially have been unsuccessful thus far, but there is still at least one possibility. The third line of attack comprises new, unconventional probe designs. We suggest several possible designs and briefly consider each. The most promising of these novel probe configurations appears to be the one based on the fiber-optic monitoring of the heating of a resistive strip, and this design is pursued in considerable detail. The idea is to deposit a thin film of some resistive metal such as nichrome on the tip of a fiber-optically sensed temperature probe. When placed in an electric field, the thin film will be heated by the induced current, and the resulting temperature rise can be measured by the temperature sensor, yielding a measure of the electric field intensity. Calculations to determine the feasibility of such a design and the optimal values of variable parameters will be presented, as will the results of some preliminary measurements.

The remainder of this report is organized as follows. The next Section is devoted to what we consider conventional approaches. We discuss the resistively tapered dipole probe and present results of preliminary measurements up to about 30 GHz. We also consider designs based on other antennas, such as the spiral. Section III deals with less conventional designs, with a heavy emphasis on the fiber-optic-thermometer based design. We also suggest several other possible designs, with an assessment of the practicality of each. Section IV contains a summary and recommendations for future work.

## II. CONVENTIONAL APPROACHES

### A. Background

Numerous configurations for electric field probes have been suggested, tested, and even marketed. It is not our intent to discuss them all here. A thorough review can be found in [3]. For present purposes it suffices to consider the two most successful and popular probe designs relevant to frequencies above 1 GHz.

The basic configuration used at NBS in developing the isotropic electric-field probe [1], and used in subsequent NBS and commercial probes, is an electrically short dipole with a diode detector (typically a beam-lead Schottky diode), connected to a metering unit by a high-resistance filter line. The small antenna(s) and high-resistance line do not perturb the fields being measured, and the transmission line does not itself pick up spurious signals and transmit them to the metering unit. For dipoles constructed from a highly conducting material, the resonant frequency of the dipole establishes an upper frequency limit for the probe since the response of the dipole becomes very frequency dependent as the resonance is approached. Thus, for example, the EFM-5 [1], which uses 5-cm dipoles (resonant frequency about 3 GHz), can only be used up to 1 GHz before its response becomes frequency dependent.

There are (at least) two ways to go to higher frequencies with this basic design. The obvious manner is to use shorter dipoles. Very small dipole probes (0.6 mm) have been used at lower frequencies for biological implantation purposes [4]. For such small antennas, however, it is not always clear that the detected signal is due to the antenna and not to spurious effects. Another way to suppress resonance effects is to use resistive dipoles rather than good conductors [5-7]. This fact can be seen quantitatively in the simple model presented in the Appendix and used in Section III. Basically the resistance reduces the magnitude of the currents induced and also damps them so that they do not persist long enough to build up a resonance. Thus for a given length dipole, one can achieve a greater frequency range by using resistive dipoles [7], but the price paid is a reduced sensitivity due to the smaller induced currents. The sensitivity loss can be ameliorated by tapering the resistive profile of the dipole [5, 6], achieving a travelling-wave antenna effect. By having the resistance grow continuously to infinity as one approaches the ends of the antenna, one can preferentially damp current reflected from the ends, thereby suppressing the resonance while not sacrificing too much sensitivity. Using resistively tapered 8-mm dipoles, a probe has been constructed which can measure 1 to 1600 V/m fields up to 18 GHz [2].

The other probe design in wide use at frequencies above 1 GHz employs a thermocouple detector to detect the temperature rise in thin resistive films [8, 9]. Use of a thin film accomplishes two purposes, as will be seen explicitly in Section III. It increases the resistance of the strip, thus increasing the heat generated (for the same amount of current). It also reduces the thermal mass of the material to be heated, thereby allowing faster response times. The geometries of the configurations used in [8] and

[9] differ, as do the methods used to obtain a cold junction in the thermocouple, but in both the hot junctions are heated by the currents induced in the junction material.

The major drawback of the thermocouple-based designs is their sensitivity to fluctuations in the ambient temperature and to other heating mechanisms. The individual thermocouple detectors are also not as sensitive as diodes, leading to the connection of many individual units in series to obtain detectable signals. That in turn raises the question of interaction between the individual units due to electromagnetic scattering. Also, because of their relatively slow response time, they cannot be used in peak or quasi-peak detectors. In their favor, probes based on thermal detection are directly sensitive to the time average of the electric field. The dipole-diode design, on the other hand, is only indirectly sensitive to the ambient temperature and has a faster response time. In the presence of waveforms more complicated than a single sinusoid, however, it does not necessarily indicate the true electric field [10]. Typically this is not a serious shortcoming if the probe is to be used as a transfer standard since such applications are usually in single-frequency cw fields. Probes based on electro-optical technology [11] promise to overcome several of the problems noted above, but they will not be operating at millimeter-wave frequencies in the near future.

Because of the success of the resistively tapered 8-mm dipole as a transfer standard up to 18 GHz, we have chosen to attempt to extend this design to higher frequencies in the hope that it can cover at least the lower portion of the frequency range of interest -- up to about 40 GHz. Results of preliminary tests and measurements are contained in the next subsection. In addition to attempting to extend the range of the resistively tapered dipole design, we also consider the possibility of using an antenna other than a dipole as the sensing element. Such an antenna would need to be broadband, of course, and it would also have to have a rather large beamwidth. The large beamwidth is necessary if it is to have any chance of serving as the basis of an isotropic probe. In the third part of this section we will consider the possibility of such an alternate antenna, with special emphasis on a cavity-backed planar spiral antenna.

## B. Resistively Tapered Dipole

The resistively tapered 8-mm probe is well documented in [2]. It consists of three orthogonal sensing elements, each of which is a resistively tapered 8-mm dipole. The resistive profile which was used for the dipoles was

$$Z(x) = \frac{60 \times 6.34 \Omega/\text{mm}}{4 \text{ mm} - |x|}, \quad |x| \leq 4 \text{ mm}. \quad (1)$$

This resistive tapering was achieved by tapering the width of the resistive strips that constitute the dipole arms, as shown in figure 1. The tapering required to eliminate reflected currents depends on the frequency, and therefore eq (1) will not be the optimal tapering for frequencies above 18 GHz.

Extension of this design to higher frequencies requires shorter dipoles with appropriate tapering for the desired frequency range (up to about 40 GHz). We are in the process of obtaining such dipoles. Preliminary tests have been performed on a 4-mm dipole obtained by cutting 2 mm off each end of an 8-mm dipole. The resulting 4-mm dipole has a resistive tapering which is not at all optimal, but measurements were made on it nonetheless to obtain a quick indication of the feasibility of this design. A Schottky diode was ultrasonically bonded across the gap, as is done in the 8-mm probe, and the frequency response was measured up to 40 GHz. This was done by immersing the unit in a 20 V/m electric field in the NBS anechoic chamber. The results of these measurements are shown in figure 2. As can be seen, the response is quite flat up to almost 30 GHz. Considering the crude tapering of the dipole, this is an encouraging result, which augurs well for the performance of a properly tapered unit.

In addition to the frequency response, a property of great interest is the antenna pattern, the angular response of the unit. For an electric dipole, the voltage across the gap should vary as  $\cos\theta$ , where  $\theta$  is the angle between the dipole axis and the polarization of the incident electric field. Any deviation from a cosine squared pattern for the voltage squared is an indication of the presence of undesirable effects, such as pickup by the leads or scattering from the substrate. Since such effects were the major obstacles in developing the 18 GHz probe, it is crucial that we check for them as we go to higher frequencies. Measurements of the angular pattern were performed at several frequencies in the anechoic chamber. A computer-driven positioner rotated the dipole, taking readings every  $8.78^\circ$ . Results of the measurements at 20 GHz and 30 GHz are shown in figure 3. The results in this case are mildly encouraging. The angular patterns could be smoother, particularly at 30 GHz, but they do exhibit a  $\cos\theta$  behavior. With a smoother resistive profile, better patterns should be achievable. In the 8-mm probe problems were encountered around 20 GHz and above due to scattering from the support to which the dipole substrates were attached. This problem was eliminated in the measurements of figure 3 by switching from a delrin support to one made of foam with a dielectric constant of 1.1 or less at these frequencies.

The results obtained with the tapered 4-mm dipole obtained by truncating an 8-mm dipole are grounds for cautious optimism. A properly tapered 4-mm unit should display better characteristics, and it therefore appears possible that it will be able to serve as the sensor for an electric-field probe covering frequencies up to about 40 GHz.

### C. Other Antennas

To cover the entire 26-110 GHz range with a single traditional antenna sensor, it is probably necessary to abandon the dipole-diode design in favor of a more broadband antenna with a correspondingly broadband detector. Patch antennas are popular in many applications at these high frequencies, but they are not suited to use in broadband probes due to their narrow bandwidth. Even patch antennas with relatively large bandwidths, such as

the electromagnetically coupled antennas [12-14], are much too narrow for our purposes.

A broadband antenna which may be suitable is the spiral. (See, e.g., [15, 16].) Spiral antennas are bidirectional unless backed by a cavity (or some other reflector). Even for an isotropic probe, unidirectionality of individual elements may be desirable in order to reduce the effect of scattering from the other antennas in the probe, and so we shall consider cavity-backed spiral antennas. The cavity reduces the bandwidth, but this disadvantage can be ameliorated somewhat by lining the cavity with absorbing material. That in turn results in a loss of power gain, but decade bandwidths are then achievable. As for the beamwidth, for a cavity-backed Archimedean spiral the beamwidth is typically between  $60^\circ$  and  $70^\circ$  at 2-5 GHz; and it is not likely to be larger at 100 GHz. That is a problem if isotropy is a concern. It would take five or six such antennas just to cover two dimensions. To cover the full  $4\pi$  solid angle would require ten to twelve spiral antennas.

The physical size of the spiral is determined by the range of frequencies it is to cover and by the tightness of the spiral ( $a$ , where the spiral is described by  $r = r_0 e^{a\phi}$ ). For efficient radiation or reception, a relatively tight spiral seems desirable,  $a \approx 0.2$ . The radius of the feed region is required to be much less than the minimum wavelength; the Antenna Engineering Handbook [17] suggests  $\lambda_{\min}/14$ . That would require an inner radius  $r_1 \leq 0.214$  mm for 100 GHz operation. Relaxing that requirement a bit would lead to a feed region of diameter  $\leq 0.5$  mm. The outer diameter of the spiral needs to be a bit bigger than  $\lambda_{\max}/\pi$ . If  $f_{\min} = 10$  GHz,  $2r_2 \geq 0.95$  cm, whereas if  $f_{\min} = 25$  GHz,  $2r_2 \geq 0.38$  cm.

Regarding the detector, most applications of spiral antennas have emphasized transmission rather than reception or use as a probe. There has been considerable difficulty developing broadband baluns at high frequency, which could pose problems for our application. For the detector, if one uses a Schottky diode as at lower frequencies, the requirements are that it be physically small (length of about 0.1 mm or less) and that its cutoff frequency exceed 100 GHz. It is not overly difficult to meet the size criterion, but the cutoff frequency could be another matter. Present detector diodes used at and above 100 GHz tend to be whisker diodes, whose mechanical instability poses a problem. An alternative would be to use thermistor detectors. It would mean sacrificing sensitivity and response time, but it might be acceptable if the required diodes could not be obtained or fabricated.

Thus far, our efforts on spiral-probe development have been directed toward locating, purchasing, and testing commercial units which operate up to 100 GHz and above. These efforts have not yet been marked by success, but the outlook is not entirely bleak.

### III. UNCONVENTIONAL PROBE CONFIGURATIONS

#### A. Design Based on Fiber-Optically Sensed Thermometer

##### A.1 General Design

The electric-field probe configuration considered in this subsection is based on a fiber-optically sensed temperature probe [18]. The temperature sensor consists of a small quantity of a phosphor affixed to the end of an optical fiber. The phosphor has the property that the lifetime of the first excited state is temperature dependent. In the temperature sensor, the phosphor is excited by a pulse of light transmitted down the fiber, and the rate of the subsequent decay back to the ground state is monitored by detecting the photons emitted and transmitted back down the fiber. The half life of the excited state determines the temperature of the phosphor and of any material with which it is in thermal equilibrium. An electric-field probe can be built around this by placing the temperature sensor in contact with a thin film of resistive material which will heat up when immersed in an electric field [19]. The resulting temperature rise is measured by the temperature sensor and gives an indication of the magnitude of the electric field. In [19] the authors used a carbon-based spray paint to paint narrow, thin crossed dipoles on polystyrene foam. The temperature probe was sandwiched between two slabs of foam with the crossed dipoles painted on one of the faces in contact with the temperature sensor.

The configuration we consider is quite different. Our idea is to deposit a thin film of a resistive material directly onto the tip of the temperature sensor, in thermal contact with the phosphor. Such a design has the advantage that it minimizes the amount of material in contact with the film which is being heated. This is important because the sensitivity of the electric field probe will depend on the amount of heat transferred to the phosphor for a given electric field. Any extra dielectric material in contact with the resistive film will absorb heat from the film, thereby reducing the amount available for the phosphor. The extra dielectric material increases the effective thermal mass which must be heated, while generating no additional heat itself. Initially it was intended that the resistive film coat the outside of the end of the fiber (about the last 1 mm) so that it formed a cylindrical tube as in figure 4a). (The phosphor would be located at the tube center.) As will be seen below, a better geometry may be a thin rectangular strip on a flat surface on the end of the sensor, figure 4b).

Calculations have been done to assess the feasibility of this design and to determine the optimal values for the various parameters. These calculations require a simple model for the power absorbed by a resistive cylinder or strip in an electric field. Such a model was previously developed in [20]. Since that work is not generally available, the model is presented here in the Appendix. In addition to the theoretical work, some preliminary measurements have been performed. Both calculations and measurements are presented below.

## A.2 Theory

The simple algebraic model (SAM), developed in [20] and presented in the Appendix, leads to the following expression for the power absorbed by a resistive tubular cylinder of length  $2\ell$  in an electric field with component  $E_z$  parallel to the axis of the cylinder,

$$P_{\text{abs}} = \frac{E_z^2 L_{\text{eff}}^2 R_{\text{abs}}}{2 |Z_{\text{in}}|^2}, \quad (2)$$

where

$$L_{\text{eff}} = \frac{2(1 - \cos k\ell)}{k \sin k\ell},$$

$$R_{\text{abs}} = \frac{R_{\text{AC}}}{2 \sin^2 k\ell} \left(1 - \frac{1}{2k\ell} \sin 2k\ell\right),$$

$$Z_{\text{in}} = R_{\text{abs}} + R_r + iX_r, \quad (3)$$

$$k = 2\pi/\lambda.$$

In eq (3)  $L_{\text{eff}}$  and  $Z_{\text{in}}$  are, respectively, the effective length and the input impedance of the cylindrical tube considered as a dipole antenna. In the equation for  $R_{\text{abs}}$ ,  $R_{\text{AC}}$  is the usual ohmic resistance.  $R_{\text{abs}}$  is an effective ohmic resistance, given the current distribution assumed on the cylinder. Since we will be dealing with resistive films which are much thinner than the skin depth of the material used,  $R_{\text{AC}}$  is given by

$$R_{\text{AC}} = \frac{\ell}{\sigma\pi R t}, \quad (4)$$

where  $\sigma$  is the conductivity of the material from which the cylinder is made,  $R$  is the radius of the cylinder,  $t$  is the thickness of the cylinder wall, and we have assumed  $t \ll R$ . The radiation resistance and reactance,  $R_r$  and  $X_r$ , are given by

$$R_r = \frac{30 \Omega}{2 \sin k\ell} \{2(1 + \cos b)S_1(b) - \cos b S_1(2b) + \sin b [\text{Si}(2b) - 2\text{Si}(b)]\},$$

$$X_r = -\frac{30 \Omega}{2 \sin k\ell} \{\sin b [\ln(\ell^2/R^2) - 2S_1(b) + S_1(2b)] - 2(1 + \cos b) \text{Si}(b) + \cos b \text{Si}(2b)\},$$

$$b = 2k\ell. \quad (5)$$

The expressions used in evaluating the sine integrals,  $S_1(b)$  and  $Si(b)$ , are given in the Appendix, as are details of the derivation of eqs (2-5).

The SAM can be used to estimate the amount of power absorbed by a resistive tubular cylinder and the consequent rate of temperature rise, and also to determine the optimum value of parameters such as  $t$  and  $\sigma$ . Beginning with parameter optimization, the first question is what quantity we wish to maximize or minimize. What will determine the sensitivity of the electric-field probe is the total amount of heat transferred to the phosphor temperature sensor for a given electric field, but that calculation would introduce dependence on too many additional parameters. The total temperature rise of the resistive film is somewhat simpler, but it is still complicated by heat-transfer problems. In order to isolate a manageable number of parameters of the resistive cylinder, we shall consider the rate of temperature rise of an isolated cylinder in an electric field. For the purpose of optimizing the parameters, neglect of the heat loss to the dielectric substrate and to the surrounding air is permitted since values that maximize the rate of temperature rise in the absence of heat loss will also maximize it in the presence of heat loss. This is because the heat-loss mechanisms do not depend on the parameters being optimized. All that will change is the actual rate of temperature rise ( $dT/d\tau$ ) achievable.

The power absorbed by a resistive cylinder was given above, eq (2). Neglecting heat loss, the rate of temperature rise is the power absorbed divided by the cylinder's mass times its specific heat capacity,

$$\frac{dT}{d\tau} = \frac{1}{4\pi\ell Rt\rho C} P_{\text{abs}}, \quad (6)$$

where  $\rho$  is the density and  $C$  the specific heat capacity (at constant pressure) of the material of the cylinder. Using the full expressions, eqs (3) and (5), for the effective length and the various contributions to the input impedance would result in an expression for  $dT/d\tau$  that was too cumbersome for analysis. We therefore resort to the approximation that the cylinder is electrically short,  $2\ell \ll \lambda$ . This approximation will be adopted only for the optimization procedure, not for the computation of power or for subsequent calculations. For  $k\ell \ll 1$  we can write

$$\begin{aligned} L_{\text{eff}} &\approx \ell, \\ R_{\text{abs}} &\approx R_{\text{AC}}/3, \\ R_{\text{r}} &\approx 20 \Omega k^2 \ell^2, \\ X_{\text{r}} &\approx -120 \Omega [\ln(\ell/R) - 0.653]. \end{aligned} \quad (7)$$

Equation (6) then takes the form

$$\frac{dT}{d\tau} \approx (\ell^2 E_z^2 / 24\pi^2 \rho C \sigma R^2 \tau^2) \left\{ \left[ \frac{\ell}{3\pi\sigma R\tau} + 20 \Omega (k\ell) \right]^2 + (120 \Omega)^2 [\ln(\ell/R) - 0.653]^2 \right\}^{-1}. \quad (8)$$

Equation (8) contains six parameters which can be adjusted to maximize the rate of temperature rise:  $\sigma$ ,  $\ell$ ,  $R$ ,  $\tau$ ,  $\rho$ , and  $C$ . Not all six are independent, however. In practice, the choice of  $\sigma$  will constrain the achievable values of  $\rho$  and  $C$ , and could even determine them uniquely. The relationship between  $C$ ,  $\rho$ , and  $\sigma$  for available materials is hopelessly complicated. To keep the problem tractable, we will treat  $C$  and  $\rho$  as constant in the optimization process. This amounts to treating them as dependent variables of  $\sigma$  and then neglecting the additional (implicit) dependence on  $\sigma$  that they introduce into eq (8). Of the remaining four variables, the optimum value for  $\ell$  can be determined by inspection: the larger  $\ell$  is, the larger  $dT/d\tau$  is. Since we want to stay below resonance, this fixes  $\ell$  to be a little less than  $\lambda/4$  at the highest frequency, or  $\lambda \approx 0.67$  mm.

Once these constraints are imposed, we are left with the problem of maximizing a function of three variables,  $\sigma$ ,  $R$ , and  $\tau$ . Except for the argument of the logarithm,  $R$  and  $\tau$  always appear in the combination  $R\tau$ . Since the logarithm is a very slowly varying function for the range of parameters we consider, as a first approximation it can be considered a constant in the maximization process. In addition to being a reasonable approximation, treating  $R$  as a constant corresponds to the actual situation, in which the cylinder radius is dictated by the radius of the temperature sensor on which the resistive film is deposited. Letting  $s = R\tau$ , the function to be minimized is then

$$\frac{dT}{d\tau}(s, \sigma) = \frac{K}{s^2 \sigma} \left[ \left( \frac{\ell}{3\pi\sigma s} + R_r \right)^2 + X_r^2 \right]^{-1}, \quad (9)$$

where  $K$ ,  $R_r$ , and  $X_r$  are all independent of  $s$  and  $\sigma$ . The function in eq (9) approaches infinity in the double limit  $s \rightarrow 0$  first, then  $\sigma \rightarrow \infty$ . There is no extremum in the finite  $s$ - $\sigma$  plane. If we consider just the finite rectangular domain  $s \in [s_{\min}, s_{\max}]$  and  $\sigma \in [\sigma_{\min}, \sigma_{\max}]$ , then the maximum of  $dT/d\tau$  over this domain occurs for

$$s = s_{\min}, \quad (10)$$

$$\sigma = \frac{\ell}{3\pi R\tau} \left\{ (20 \Omega k^2 \ell^2)^2 + (120 \Omega)^2 [\ln(\ell/R) - 0.653]^2 \right\}^{-1/2}.$$

The value of  $\sigma$  corresponds to the requirement that  $R_{\text{abs}}^2 = R_r^2 + X_r^2$ . Physically what is happening is that for a fixed thickness and radius if  $\sigma$  is made too small then very little current is induced and very little heat is generated, whereas if  $\sigma$  is very large then the induced current is also large, but the generated heat is again small because of the small ohmic resistance. The

optimum value of the conductivity is somewhere between the two extremes, and it happens to be the value for which the effective ohmic resistance ( $R_{abs}$ ) is equal to the radiation impedance of the cylinder. Thus, to maximize the rate of temperature rise of the cylinder -- which with our assumptions is the same as maximizing the power absorbed per unit volume -- we should use the smallest possible value of the product  $R \times t$  and then choose the conductivity according to eq (10).

What then is the maximum rate of temperature rise that can be achieved? For a given radius and thickness, the optimal conductivity can be computed from eq (10) and then substituted into eq (9) to obtain the rate of temperature rise. In figure 5 the rate of temperature rise in a 1 V/m, 40 GHz field is plotted as a function of the thickness  $t$  for fixed radius,  $R = 0.5$  mm. Representative values for the optimal conductivity used to obtain these rates are  $\sigma = 2.72 \times 10^4$  S/m for  $t = 100$  nm and  $\sigma = 2.72 \times 10^5$  S/m for  $t = 10$  nm. In obtaining these results, the values  $C = 377$  J/(kg K) and  $\rho = 8 \times 10^3$  kg/m<sup>3</sup> were used. These correspond to the approximate specific heat capacity and density of bulk nichrome. Nichrome was considered the appropriate material because the optimal conductivities were found to be close to the conductivity of bulk nichrome. It should be noted that the conductivity of thin-film nichrome is not necessarily equal to that of bulk nichrome. This will be noted further in the discussion of the preliminary measurements. The temperature rises displayed in figure 5 are not terribly encouraging. Even if a coating thickness of 10 nm can be achieved, and if the optimal conductivity is used, the temperature will rise at the rate of only 0.009 K/s in a 1-V/m field, which would be quite difficult to measure in a bulk material, and almost certainly impossible in a thin film. A 10-V/m field, however, would result in a 100-fold increase in the power absorbed and the rate of temperature rise.

The amount of power absorbed by the resistive cylinder is also of considerable interest, since once the cylinder has reached its equilibrium temperature any power absorbed will be transferred to either the surroundings (air, substrate) or to the temperature sensor. The power absorbed, therefore, places an upper limit on the amount of power transferred to the temperature sensor. In addition to the magnitude of the power absorbed, we must know its frequency dependence. If the electric-field probe is to be frequency independent, the power absorbed must be independent of the frequency of the incident radiation. In figure 6 we plot the power absorbed by a resistive cylinder as a function of frequency for three sets of cylinder parameters:  $[\sigma(\text{S/m}), t(\text{nm})] = (10^4, 10), (10^5, 10),$  and  $(10^5, 100)$ , all with  $2\ell = 1$  mm and  $R = 0.25$  mm. In each case the conductivity used is optimal given the values of  $R$  and  $t$ . The absorbed power was computed from eqs (2-5). The electrical shortness approximations, eq (7), were not made in this computation. Instead, the full expressions for the effective length and input impedance, eqs (3-5), were used. Figure 6 contains good news and bad news. The good news is that a very flat frequency response is predicted for a coating thickness of 10 nm. The bad news is that the amount of power absorbed is miniscule, about one half

nanowatt. This will probably be insufficient to heat the phosphor appreciably. Furthermore, it may not be possible to obtain a film as thin as 10 nm.

As an alternative to the resistive cylinder, we also consider a thin, flat, resistive strip on a dielectric substrate. We do so because it may prove to be a better configuration, and because it corresponds to the geometry used in the preliminary measurements to be discussed below. The expression for the power absorbed by such a resistive strip in an electric field is the same as that for the resistive cylinder, eq (2), except that the input impedance,  $Z_{in}$ , is different. Equation (4) holds as before, but eqs (4) and (5) must be modified. For the resistive strip of length  $\ell$ , thickness  $t$ , and width  $w$ ,  $R_{AC}$  is given by

$$R_{AC} = \frac{2\ell}{\sigma w t} . \quad (11)$$

King has shown [21] that for a cylindrical dipole of noncircular cross section the radiation resistance can be obtained from that of a circular cylindrical dipole with an equivalent radius which depends on the dimensions and cross sectional shape of the dipole of interest. For a very thin, narrow, rectangular cross section the effective radius is one fourth of the width. This is obtained by considering the thin rectangular cross section as a highly eccentric ellipse, so that

$$R_{eff} = \frac{1}{2} (a_e + b_e) \approx a_e/2 = w/4, \quad (12)$$

where  $a_e$  and  $b_e$  are the major and minor radii of the ellipse [21, 22]. The derivation of this result assumed that the width is much less than the length of the dipole, which will not be the case in the applications below. This approximation, therefore, is suspect, but we shall use it nonetheless to obtain an indication of the size of the input impedance for the resistive strip configuration. The approximate input impedance of the resistive strip is given by eqs (3), (5), and (11), with the radius  $R$  replaced by the effective radius of eq (12). The power absorbed in an electric field can then be computed from eq (2) and compared to the result for a circular cylindrical dipole. Figure 7 plots the absorbed power in a 1-V/m field for thin-film tubular and strip dipoles of two different thicknesses. The length, thickness, specific heat capacity, density, and conductivity were chosen to be the same as in figure 6. The strip width was taken to be 0.5 mm, and the tube radius was  $R=(0.5/2\pi)$  mm so that equal amounts of material are present in strip and tube.

Two features stand out in figure 7. The strip configuration absorbs more power, and it also has a flatter frequency response. Both effects are small for the 10 nm thickness, but are quite pronounced for 100 nm. Both features are due to the smaller radiation impedance, particularly the radiation reactance, of the strip as compared to the tube. The ohmic resistance is the same for the two configurations, but for the tube the

radiation impedance is comparable to the ohmic resistance, whereas for the strip the radiation impedance is considerably smaller. Consequently, the tube has less current induced and less heat generated (since same ohmic resistance). Furthermore, the power absorbed by the tube will also reflect the resonant behavior of the radiation impedance and will therefore be more frequency dependent. Because of its slightly better behavior, we are led to choose the rectangular strip configuration over the tubular cylinder as the sensing component of the probe.

Thus far we have neglected the effect of the dielectric on which the thin films are deposited -- the fiber filling the middle of the tubular cylinder and the substrate on which the resistive strip resides. Ideally, we would like them to have no effect on the response of the thin film, but it is necessary to check whether this is the case. The effect of the dielectric substrate on the power absorbed by a rectangular strip is the easier of the two to analyze, and so we consider that case. The substrate is assumed to have large transverse dimensions so that it can be approximated by an infinite slab of thickness  $d$ . We wish to calculate the field just outside the dielectric when a plane wave of amplitude  $E_0$  is normally incident. This is a standard problem in boundary-condition matching, whose solution is

$$E = E_0 \left( 1 - \frac{\epsilon - 1}{\epsilon + 1 + 2i\sqrt{\epsilon} \cot k'd} \right), \quad (13)$$

where  $k'$  is the wave number in the dielectric. To assess the size of this effect, we plot in figure 8  $\rho = E/E_0$  for  $\epsilon = 4$  and  $5$ , which are typical values for glass. Two disturbing features are evident in figure 8. The dielectric substrate decreases the field by as much as 60% at some frequencies, with a corresponding decrease in the minimum field level that can be detected. Even more serious is the fact that the effect is frequency dependent. A frequency variation of  $\pm 4$  dB or more, as in figure 8b), is unacceptable. The permittivity of the substrate cannot be made small since we wish to deposit the thin film on the tip of the temperature sensor. Therefore, the only way to eliminate the frequency dependence introduced by the substrate is to make it much thinner than a wavelength. This may be achievable by using a tapered tip for the temperature sensor. If the thickness of the dielectric cannot be made small, the frequency dependence evident in figure 8 would seem to rule out this design for a broadband probe.

### A.3 Exploratory Experiment

In the theory section above, we avoided detailed consideration of heat-transfer mechanisms and the actual rise in the equilibrium temperature of the resistive structures in electric fields. To address this question, as well as to test the general feasibility of this approach, an experiment was designed and conducted. Rectangular strips ( $2 \text{ mm} \times 1 \text{ mm}$ ) of nichrome were deposited on 1-cm square slabs of glass. The thickness of the nichrome film was not measured during deposition; it is believed to be between 10 and 100 nm. Two sets of samples were made, one with surface resistivities ranging from  $740 \text{ } \Omega/\text{sqr}$  (i.e. the resistance across a square section is  $740 \text{ } \Omega$ ) to  $850$

$\Omega/\text{sqr}$ , and the other with 3.1 to 3.9  $\text{k}\Omega/\text{sqr}$ . Because the strips are so thin the conductivity of the strip is not that of bulk nichrome, and the thickness cannot be inferred from the surface resistivity. The glass substrates are about 1 mm thick. The length and width of the strips were chosen to be about two to three times the dimensions which would be used for frequencies up to 110 GHz. This scaling was done so that measurements in the NBS anechoic chamber, which only extend to 40 GHz at present, could be scaled up to the frequency range of interest.

The samples were irradiated with electric fields parallel to their lengths, and their temperature was monitored by the fiber-optically sensed temperature probe described above and in [18]. Initial measurements were made in a small, portable, absorber-lined chamber at 20 GHz. No detectable temperature rise was observed, even for field levels as high as 300 V/m ( $24.35 \text{ mW/cm}^2$ ). The sensitivity of the temperature sensor was limited by fluctuations in the ambient temperature, which were approximately 0.3 K.

Additional measurements were made in the anechoic chamber at 16 GHz. With no incident field, the temperature was measured to be  $22.5 \pm 0.4$  °C. For an electric field of 658 V/m, the temperature rose to  $23.7 \pm 0.2$  °C. When the field was turned off, the temperature fell back to its initial range. These measurements were performed on a sample with surface resistivity 3.7  $\text{k}\Omega/\text{sqr}$ . A larger effect was observed with a sample with 780  $\Omega/\text{sqr}$ . In an electric field of 662 V/m, the temperature rose to  $23.5 \pm 0.4$  °C from an ambient of  $21.5 \pm 0.2$  °C.

To test whether the effect observed was due to the heating of the resistive strip and not to the dielectric substrate, measurements were also made on a plain glass slab without a thin film present. At 16 GHz, for a 658 V/m electric field, the temperature rose to  $23.0 \pm 0.2$  °C from an ambient of  $21.5 \pm 0.2$  °C. Comparing this with the results above indicates that the entire temperature rise observed in the resistive-strip samples could have been due to the generation of heat in the dielectric substrate rather than in the thin film. We also tested the temperature sensor alone in the electric field and observed no effect. This is to be expected since in the experimental configuration the fiber of the sensor is oriented perpendicular to the field.

In the measurements above, the time it took for the sample (with or without thin film) to reach its equilibrium temperature after the field was turned on was about one to two minutes. Such a slow characteristic time indicates that it is the thermal mass of the glass, rather than of the film, that is controlling the rate of heating. This fact is confirmed by other measurements made with the infrared camera system of Professors Norgard and Sega at the University of Colorado at Colorado Springs. This system has sufficient resolution to see the temperature distribution across the sample, showing whether the entire glass slab or only the resistive film is heating. At field levels sufficient to heat the sample, it was observed that the

temperature of the entire substrate rose, indicating that either the heat transfer between film and substrate was sufficient for the film to heat the substrate, or that the substrate was heated directly from absorbed radiation.

#### A.4 Summary

The theory and results of preliminary measurements indicate that there are several sizeable obstacles which must be overcome before this probe design can be considered feasible. The overriding problem is to obtain an observable heating effect in the resistive strip for reasonable field levels. Even if the heating effect observed in the measurements so far is due in part to the resistive strip, which is possible but not certain, an improvement of about four orders of magnitude in (power) sensitivity would be needed. Two ways in which an actual probe would achieve sensitivity improvements over the preliminary experiments are clear. The present temperature sensor is in principle capable of measuring temperature rises of 0.1 K, and improved models are expected to be able to measure 0.01 K, but the measurements described above were limited by fluctuations in the ambient temperature of order 0.3 K. In the probe design the resistive strip could be thermally insulated from the ambient, thus eliminating these fluctuations and allowing smaller temperature changes to be observed. Another tactic to subtract the ambient-temperature fluctuations would be to use two temperature sensors, one with the resistive film and one without. The uncoated sensor would respond to ambient fluctuations, which could then be subtracted, provided the fluctuations did not vary significantly over the distance between the two sensors.

The sensitivity would also be increased due to the smaller effective thermal mass of the probe configuration compared to the experimental setup. In the experiment, the 2 mm<sup>2</sup> thin film was in thermal contact with the 0.1 cm<sup>3</sup> volume of glass substrate, whereas in a probe there would only be of order 1 mm<sup>3</sup> of optical fiber and phosphor to be heated by a film of about the same surface area. Another possible source of increased sensitivity would be improvements in the temperature sensor, which are quite possible.

If reasonable field levels can be made to produce observable effects, the next problem would be to eliminate the frequency dependence introduced by the dielectric on which the film resides -- the glass slab in the experiment and the fiber in the actual probe. The obvious way to achieve this would be to use a thinner substrate/fiber. It might also be possible to reduce the effect by using a different geometry, such as a rectangular strip on a wedge-shaped sensor tip, as mentioned earlier and shown in figure 4b).

A problem which will remain, even if all the aforementioned difficulties can be resolved, is the fact that this is a thermometric design, and as such it is subject to the problems of all such designs: variations in the ambient, drift during continuous use, and the like.

## B. Other Unconventional Probe Configurations

In addition to the probe design described in the preceding subsection, several other designs were considered and subsequently discarded. We note them briefly here.

If a phosphor which would itself heat in an electric field could be found, the probe design of Section III.A could be simplified to a strip of phosphor whose temperature was monitored optically, eliminating the need for the resistive strip and the problem of transferring sufficient heat from strip to phosphor to heat the phosphor. This avenue has not been explored at this time.

The idea of a semiconductor probe in which the incident radiation would raise additional electrons to the conduction band was dismissed because characteristic thermal energies at room temperature are about 60 times larger than the energy of a 100-GHz photon. Consequently, even if a material could be found with the correct band gap, the conduction band would already be populated at room temperature.

The birefringence of lithium tantalate crystals is temperature dependent. By coating such a crystal with an absorptive material, one could hope to measure the temperature change of the material in an electric field by monitoring the birefringence of the crystal. One immediate problem would be how to heat the entire crystal uniformly. If that could be overcome, the sensitivity of such a device could be sufficient. For a crystal of 1 mm length, we would expect a full cycle shift for a temperature rise of about 5 K. Since shifts of 0.01 of a full cycle can be detected, this would allow detection of temperature changes of about 0.05 K, which is competitive with other thermal detection methods, and which could be improved further by detecting smaller fringe shifts. A thermometer based on this concept has, in fact, been developed [23].

Another optics-based idea for thermal detection is to measure the thermal expansion of a lossy material by use of a Fabry-Perot interferometer. Again, however, the sensitivity does not match that of other thermal detection methods. Using representative values for thermal expansion coefficients and assuming an expansion of one tenth of a wavelength is detectable one concludes that a temperature rise of 16 K is required to obtain a detectable expansion.

## IV. SUMMARY AND RECOMMENDATIONS

Development of an electric-field probe to cover the frequency range 26-110 GHz does not promise to be a simple task. The results obtained thus far with the resistively tapered dipole design are encouraging, and it appears probable that this design can be extended to cover the bottom of the frequency range of interest, up to 30 or 40 GHz. Beyond that, however, the picture darkens considerably. It is not clear that suitable high-frequency broadband antennas and detectors are available commercially, which makes the development of a conventional probe design for these frequencies very

difficult. The most promising unconventional design, based on the optically-sensed temperature sensor, has major problems which must be overcome before it can be considered a real possibility. Since there is a definite need for electric-field probes in the millimeter-wave range, we recommend the following.

- 1) The resistively tapered dipole design should be extended to the highest frequency possible. This will involve fabrication of properly tapered 4-mm and 2-mm thin-film dipoles, identification and purchase of suitable diode detectors, assembly of components, and testing, characterization, and calibration of the units.
- 2) Efforts to obtain high-frequency broadband antennas commercially should continue. If they can be obtained, their frequency response and beamwidth need to be measured and suitable detectors obtained and tested before final design of a probe based on the antennas can be done.
- 3) Investigation of the design based on the optically-sensed thermometer should continue. The next step would be to make further measurement, using thin-films on smaller substrates in a more stable thermal environment. If these are successful, the choice of geometry (cylindrical or rectangular strip) must be made, and a thin film should be deposited on a temperature sensor and tested.

#### REFERENCES

- [1] Larsen, E. B.; Ries, F. X. Design and calibration of the NBS isotropic electric-field monitor (EFM-5), 0.2 to 1000 MHz, NBS Tech. Note 1033, March 1981.
- [2] Kanda, M.; Driver, L. D. An Isotropic electric-field probe with tapered resistive dipoles for broad-band use, 100 kHz to 18 GHz, IEEE Trans. MTT-35, no. 2, 124-130, February 1987.
- [3] Tell, R. A. Instrumentation for measurement of radiofrequency electromagnetic fields: equipment, calibrations, and selected applications, in Proceedings of a NATO Advanced Study Institute in biological effects and dosimetry of low energy electromagnetic fields, M. Grandolfo, S. Michaelson, and A. Rindi, eds. New York: Plenum, 1983.
- [4] Batchman, T. E.; Gimpelson, G. An implantable electric-field probe of submillimeter dimensions, IEEE Trans. MTT-31, no. 9, 745-751, September, 1983.
- [5] Wu, T. T.; King, R. W. P. The Cylindrical antenna with nonreflecting resistive loading, IEEE Trans. AP-13, no. 3, 369-373, May 1965.
- [6] Kanda, M. A Relatively short cylindrical broad-band antenna with tapered resistive loading for picosecond pulse measurements, IEEE Trans. AP-26, no. 3, 439-447, May 1978.
- [7] Hopfer, S.; Adler, Z. An Ultra broad-band (200 kHz-26 GHz) high-sensitivity probe, IEEE Trans. IM-29, no. 4, 445-451, December 1980.
- [8] Aslan, E. Broad-band isotropic electromagnetic radiation monitor, IEEE Trans. IM-21, no. 4, 421-424, November 1972.

- [9] Hopfer, S. The Design of broad-band resistive radiation probes, IEEE Trans. IM-21, no. 4, 416-421, November 1972.
- [10] Randa, J.; Kanda, M. Multiple-source, multiple-frequency error of an electric field meter, IEEE Trans. AP-33, no. 1, 2-9, January 1985.
- [11] Chang, J., ed. High bandwidth analog applications of photonics, Proc. SPIE 720, 1970.
- [12] Hall, P. S.; Wood, C.; Garrett, C. Wide bandwidth microstrip antennas for circuit integration, Electronics Lett. 15, no. 15, 458-460, July 1979.
- [13] Suzuki, Y.; Miyano, N.; Chiba, T. Expanding the frequency bandwidth of a microstrip antenna, IEEE AP-S 1981 International Symposium Digest, 366-369, June 1981.
- [14] Sabban, A. A New broadband stacked two-layer microstrip antenna, IEEE AP-S 1983 International Symposium Digest, 63-67, May 1983.
- [15] Dyson, J. D. The Equiangular spiral antenna, IRE Trans. AP-7, 181-187, April 1959.
- [16] Rumsey, V. H. Frequency independent antennas. New York, NY: Academic Press, 1966.
- [17] Deschamps, G. A.; DuHamel, R. H. Frequency-independent antennas, in Antenna Engineering Handbook, ed. H. Jasik; New York, NY: McGraw-Hill, 1961.
- [18] Wickersheim, K. A.; Sun, M. H. Fluoroptic thermometry, Measurement and Control, p. 132, June 1987.
- [19] Martin, V. M.; Sega, R. M.; Durham, R. Fiber optic microwave power probe, Optical Eng. 26, no. 2, 170-173, February 1987.
- [20] Randa, J. Reflection and absorption properties of a sparse, planar, random array of lossy wires; unpublished report to sponsor, January 1987.
- [21] King, R. W. P. Chapter 1 in The Theory of linear antennas. Cambridge, MA: Harvard University Press, 1956.
- [22] Elliot, R. S. Chapter 7.12 in Antenna theory and design. Englewood Cliffs, NJ: Prentice-Hall, 1981.
- [23] Cetas, T. C. A birefringent crystal optical thermometer for measurements of electromagnetically induced heating, in Biological effects of waves, Vol. II, C. C. Johnson and M. L. Shore, eds. Rockville, MD: HEW Publ. (FDA) 77-8011, 1977, pp.338-348.
- [24] Pistolkors, A. A. The Radiation resistance of beam antennas, Proc. I.R.E. 17, no. 3, 562-579, March 1929.
- [25] Stratton, J. A. Chapter 8 in Electromagnetic theory. New York, NY: McGraw-Hill, 1941.
- [26] Jordan, E. C.; Balmain, K. G. Chapter 14 in Electromagnetic waves and radiating systems. Englewood Cliffs, NJ: Prentice-Hall, 1968.
- [27] Einarsson, O. Chapter 12 in Electromagnetic and acoustic scattering by simple shapes, J. J. Bowman, T. B. A. Senior, and P. L. E. Uslenghi, eds. Amsterdam, The Netherlands: North Holland, 1969.
- [28] Cassedy, E. S.; Fainberg, J. Back scattering cross sections of cylindrical wires of finite conductivity. IRE Trans. AP-8, no. 1, 1-7, January 1960.

## APPENDIX

We consider a hollow, circular cylinder of length  $2\ell$  and radius  $R$ , with a thickness  $t$  and conductivity  $\sigma$  (fig. 9). The radius is much smaller than the length and the wavelength of the incident radiation and is much larger than the thickness:  $\lambda, 2\ell \gg R \gg t$ . To treat the scattering from and absorption by such a cylinder we assume a sinusoidal current distribution along its length,

$$I(x) = I_m \sin[k(\ell - |x|)], \quad (\text{A.1})$$

and use a simple algebraic method to compute the amplitude of the induced current,  $I_m$ , or equivalently the current at the midpoint of the cylinder,  $I(0)$ . The simple algebraic method (SAM) is based on the EMF method, as found, e. g., in [24-26]. The current at the midpoint of the wire,  $I(0)$ , is the short-circuit current for a receiving dipole. It is given by

$$I(0) = \frac{E_x L_{\text{eff}}}{Z_{\text{in}}}, \quad (\text{A.2})$$

where  $E_x$  is the component of the incident field parallel to the dipole, cf. figure 9b), and we have assumed that the incident field does not vary along the length of the dipole.  $Z_{\text{in}}$  is the input impedance of the dipole used in the transmitting mode, and  $L_{\text{eff}}$  is the effective length. The effective length is given by

$$L_{\text{eff}} \equiv \frac{1}{I(0)} \int_{-\ell}^{\ell} I(x) dx = \frac{2}{k} \frac{(1 - \cos k\ell)}{\sin k\ell}. \quad (\text{A.3})$$

The input impedance  $Z_{\text{in}}$  has three components--the radiation resistance, the radiation reactance, and a contribution from the ac resistance. The radiation resistance ( $R_r$ ) and reactance ( $X_r$ ) of a center-fed tubular dipole with sinusoidal current distribution are well known [26],

$$\begin{aligned} R_r &= \frac{30 \Omega}{2 \sin k\ell} \{ 2(1 + \cos b) S_1(b) - \cos b S_1(2b) + \sin b [\text{Si}(2b) \\ &\quad - 2 \text{Si}(b)] \}, \\ X_r &= - \frac{30 \Omega}{2 \sin k\ell} \left\{ \sin b \left[ -\gamma + \ln\left(\frac{\ell}{2}\right) + 2 \text{Ci}(b) - \text{Ci}(2b) \right] \right. \\ &\quad \left. - 2(1 + \cos b) \text{Si}(b) + \cos b \text{Si}(2b) \right\}, \end{aligned} \quad (\text{A.4})$$

where

$$b = 2k\ell, \quad k = 2\pi/\lambda, \quad \gamma = 0.5772147\dots$$

The sine and cosine integrals have convenient series representations (for computational purposes),

$$\begin{aligned} \text{Si}(x) &\equiv \int_0^x \frac{\sin v}{v} dv = \sum_{n=0}^{\infty} \frac{(-1)^n x^{2n+1}}{(2n+1)(2n+1)!}, \\ \text{S}_1(x) &\equiv \int_0^x \frac{1 - \cos v}{v} dv = - \sum_{n=1}^{\infty} \frac{(-1)^n x^{2n}}{2n(2n)!}, \\ \text{Ci}(x) &\equiv - \int_x^{\infty} \frac{\cos v}{v} dv = \ln x + \gamma - \text{S}_1(x). \end{aligned} \tag{A.5}$$

Use of eq (A.5) allows us to simplify the expression for  $X_r$  slightly,

$$\begin{aligned} X_r &= - \frac{30 \Omega}{2 \sin k\ell} \{ \sin b [\ln(\ell^2/R^2) - 2 \text{S}_1(b) + \text{S}_1(2b)] - 2(1 + \cos b) \text{Si}(b) \\ &\quad + \cos b \text{Si}(2b) \}. \end{aligned} \tag{A.6}$$

Because we shall be dealing with cylinder thicknesses that are much smaller than the skin depth at the relevant frequencies, the ac impedance per unit length of the cylinder is entirely resistive and is given by its dc value,

$$\frac{1}{2\ell} R_{AC} = \frac{1}{\sigma 2\pi R t}. \tag{A.7}$$

$R_{AC}$  cannot be added directly to the radiation input impedance.  $R_{AC}$  relates current to voltage for a uniform current distribution, which is not the present case. The voltage drop across the length of wire for the current distribution given in eq (A.1) is

$$\begin{aligned} \Delta V &= \int_{-\ell}^{\ell} \left( \frac{1}{2\ell} R_{AC} \right) I_m \sin[k(\ell - |x|)] dx \\ &= \frac{I_m}{2} R_{AC} \left( 1 - \frac{1}{2k\ell} \sin 2k\ell \right) \\ &= I(0) R_{abs}, \end{aligned} \tag{A.8}$$

where

$$R_{abs} \equiv R_{AC} \frac{1}{2 \sin k\ell} \left( 1 - \frac{1}{2k\ell} \sin 2k\ell \right). \tag{A.9}$$

Since  $Z_{in}$  relates the voltage applied at the terminals of the dipole to the input current  $I(0)$ ,  $R_{abs}$  is the contribution to  $Z_{in}$  from  $R_{AC}$ . We can therefore write  $Z_{in}$  as

$$Z_{in} = R_{abs} + R_r + i X_r, \quad (A.10)$$

with  $R_r$ ,  $X_r$ , and  $R_{abs}$  given by eqs (A.4) and (A.9).

Having determined  $L_{eff}$ , eq (A.3), and  $Z_{in}$ , eq (A.10), we know  $I(0)$  from eq (A.2) for a given incident field  $E_x$ . That enables us to write the power absorbed and power scattered by the resistive tubular cylinder,

$$P_{scat} = \frac{1}{2} |I(0)|^2 R_r = \frac{1}{2} \frac{E_x^2 L_{eff}^2}{|Z_{in}|^2} R_r, \quad (A.11)$$

$$P_{abs} = \frac{1}{2} |I(0)|^2 R_{abs} = \frac{1}{2} \frac{E_x^2 L_{eff}^2}{|Z_{in}|^2} R_{abs}.$$

The scattered power is the power that is reradiated by the current induced in the cylinder, and the absorbed power is the power dissipated in ohmic heating. The powers in eq (A.11) are time averages, whereas  $E_x$  is the amplitude of the x component of the incident wave. Note that although the expressions for  $L_{eff}$ ,  $Z_{in}$ ,  $R_r$ , and  $R_{abs}$  all diverge for  $\sin k\ell \rightarrow 0$ , they enter eq (A.11) in such a combination that the powers remain finite.

Equation (A.11) is what we shall need in our analysis of the heating of a resistive cylinder. Before using the model, however, we should check that it is reasonable. To do so, we use the model to calculate the radar cross section (RCS) of resistive wire and compare it to published results, both experimental and theoretical. A review of the RCS results for lossless wires can be found in Einarsson's chapter of [27], which also contains references to the original papers. Figure 10 (taken from figure 12.8 of [27]) represents theoretical and experimental results of interest to us. The curves represent calculation results, and the circles are measured points. The quantity  $L$  is defined as  $2\pi\ell/\lambda$ , so that the resonances at  $L = (2n + 1)\pi/2$  correspond to  $2\ell = (2n + 1)\lambda/2$ . The general features are clear: a first resonance at  $2\ell \approx \lambda/2$ , with a peak value of  $\sigma/\lambda^2 \approx 0.8-0.9$ , followed by a plateau with  $\sigma/\lambda^2 \approx 0.1-0.2$ , a second resonance at  $2\ell \approx 3\lambda/2$ , a second (higher) plateau, and so on. Calculations and measurements have also been done for lossy wires [28]. In figure 11 we reproduce their figure 10, which plots the RCS for lossless wires (theory) and for a particular lossy wire (theory and experiment). The lossless result resembles that of figure 10,

as it should, and for the lossy wire theory and experiment agree quite well. The lossy wire that was used had an ac resistance of 2800  $\Omega$ /m. For a resonant length of  $2\ell = 5$  cm (3 GHz), the wire had a resistance of 140  $\Omega$ . The effect of the resistance is to decrease the resonant RCS by a factor of about four. In addition, the resonance becomes broader. These two trends, the resonance becoming lower and broader, continue as the resistance is increased, until the resonance is washed out altogether.

We now turn to calculations of the RCS using the simple model described above. The RCS is defined as the effective area required to intercept an amount of power equal to  $4\pi R^2$  times the backscattered ( $\theta = 180^\circ$ ) power per unit area for a given incident field,

$$\text{RCS} = \lim_{R \rightarrow \infty} \frac{\frac{dP}{dA}(\theta=\pi)}{\left(\frac{dP}{dA}\right)_{\text{inc}}} \times 4\pi R^2. \quad (\text{A.12})$$

(The quantity  $4\pi R^2$  times the backscattered power per unit area is just the total power scattered assuming isotropic scattering.) Equation (A.11) gives the total power scattered by a (tubular) wire; to obtain the RCS we need only relate that to the power density scattered back to the source. The angular distribution of the power radiated or scattered by an electric dipole is

$$\frac{dP}{dA}(r, \theta, \phi) = \frac{C}{r^2} \frac{\cos^2\left(\frac{\pi}{2}\cos\theta\right)}{\sin^2\theta}, \quad (\text{A.13})$$

where C is related to the total scattered power by integrating over the surface of the sphere,

$$P_{\text{scat}} = \int \frac{dP}{dA} dA = 4\pi (0.6093) C. \quad (\text{A.14})$$

Equations (A.13) and (A.14) can be used in eq (A.12) to write the RCS in terms of the total scattered power for an electric dipole,

$$\text{RCS} = \frac{P_{\text{scat}}}{0.6093\left(\frac{dP}{dA}\right)_{\text{inc}}}. \quad (\text{A.15})$$

Using eq (A.11) for  $P_{\text{scat}}$  and writing the incident power density in terms of the incident electric field, we have

$$\left(\frac{dP}{dA}\right)_{\text{inc}} = \frac{1}{2} \frac{E_i^2}{\eta}, \quad \eta = 377 \Omega, \quad (\text{A.16})$$

$$\text{RCS} = 1.641 L_{\text{eff}}^2 \eta R_r / |Z_{\text{in}}|^2.$$

Equation (A.16) is the expression for the RCS of a tubular cylinder in our SAM, with  $R_r$  and  $Z_{\text{in}}$  determined by eqs (A.5), (A.9), and (A.10) and  $L_{\text{eff}}$  by eq (A.4). To compare to the results of figure 11, we use a cylinder radius of  $12.7 \mu\text{m}$ . This is the same as was used in obtaining figure 11, so that capacitive effects will be the same. The material of the cylinder is taken to be silver ( $\sigma = 6.17 \times 10^7 \text{ S/m}$ ), and a thickness of  $72.5 \text{ nm}$  is used. This yields a fiber with an ac resistance of  $2802 \Omega/\text{m}$ , compared to the  $2800 \Omega/\text{m}$  bismuth wire used in figure 11. To generate predictions for the lossless case, we assume a solid silver wire of radius  $12.7 \mu\text{m}$ , by taking  $2\pi R t \rightarrow \pi R^2$  in eq (A.7). This yields a wire with  $32 \Omega/\text{m}$ , which is close enough to lossless for our purposes. Figure 12 displays our predicted RCS for these two cases, which should be compared to the curves of figure 11. The agreement is excellent for both the lossless and the lossy cases. The location, height, and width of the resonances all agree very well with the curves in figure 11, which represent the results of more exact calculations and of measurements. The success of the SAM in predicting the RCS for both the lossless and the lossy wires gives us confidence in its ability to predict scattering and absorption of lossy wires with different parameters.

We should note the limitations of the model in predicting the RCS of wires. If we consider higher frequencies than those represented in figs. 11 and 12, problems are encountered. In particular, a spurious maximum occurs just above  $2\ell/\lambda = 1$ . Consequently, the model should not be used above about  $2\ell/\lambda = 0.8$ . It can, however, be trusted through the first resonance, for the location and strength of that resonance, and for the height of the plateau after the resonance.

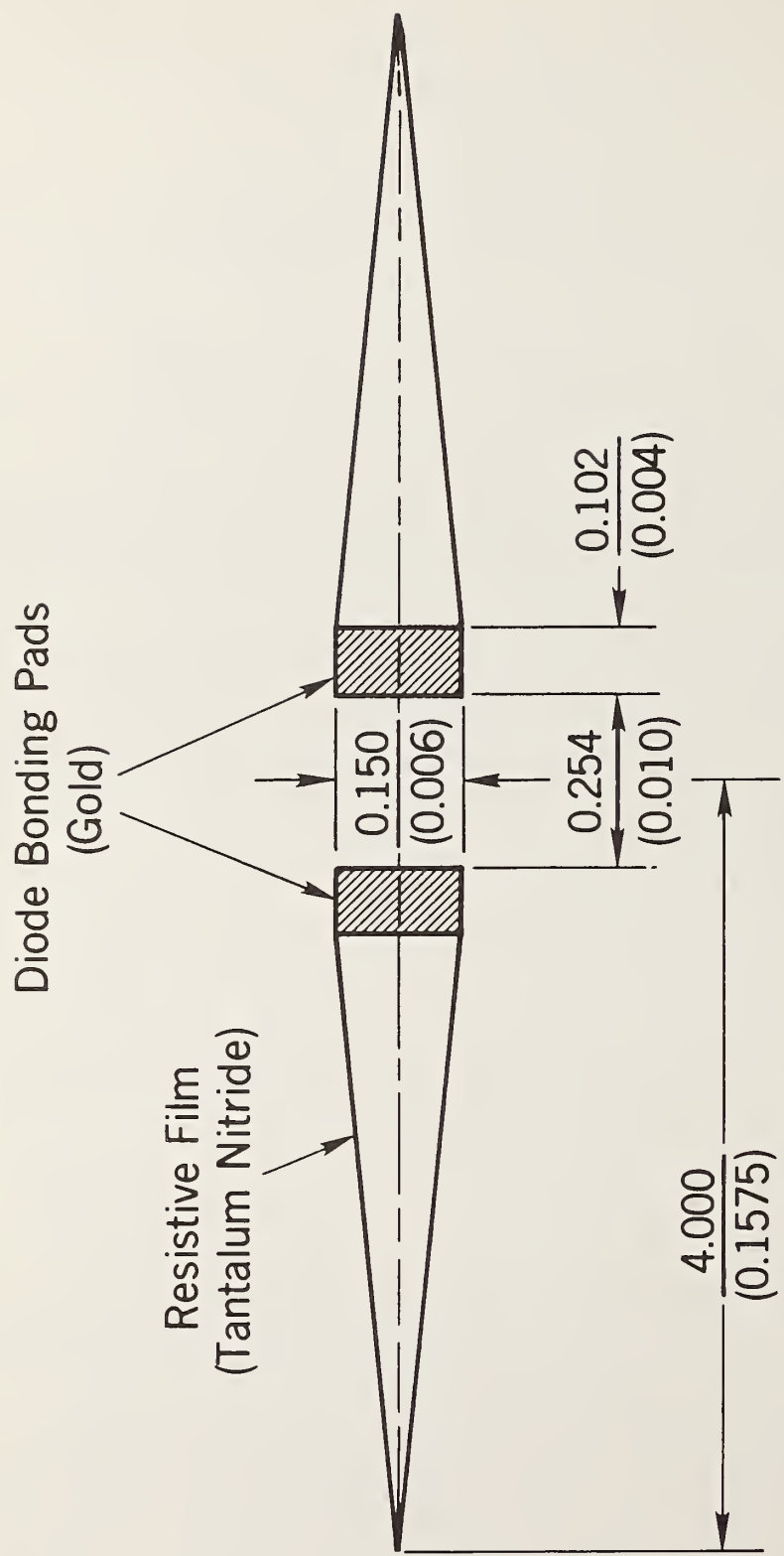


Figure 1 The 8-mm resistively tapered dipole element. Dimensions are in millimeters (and inches).

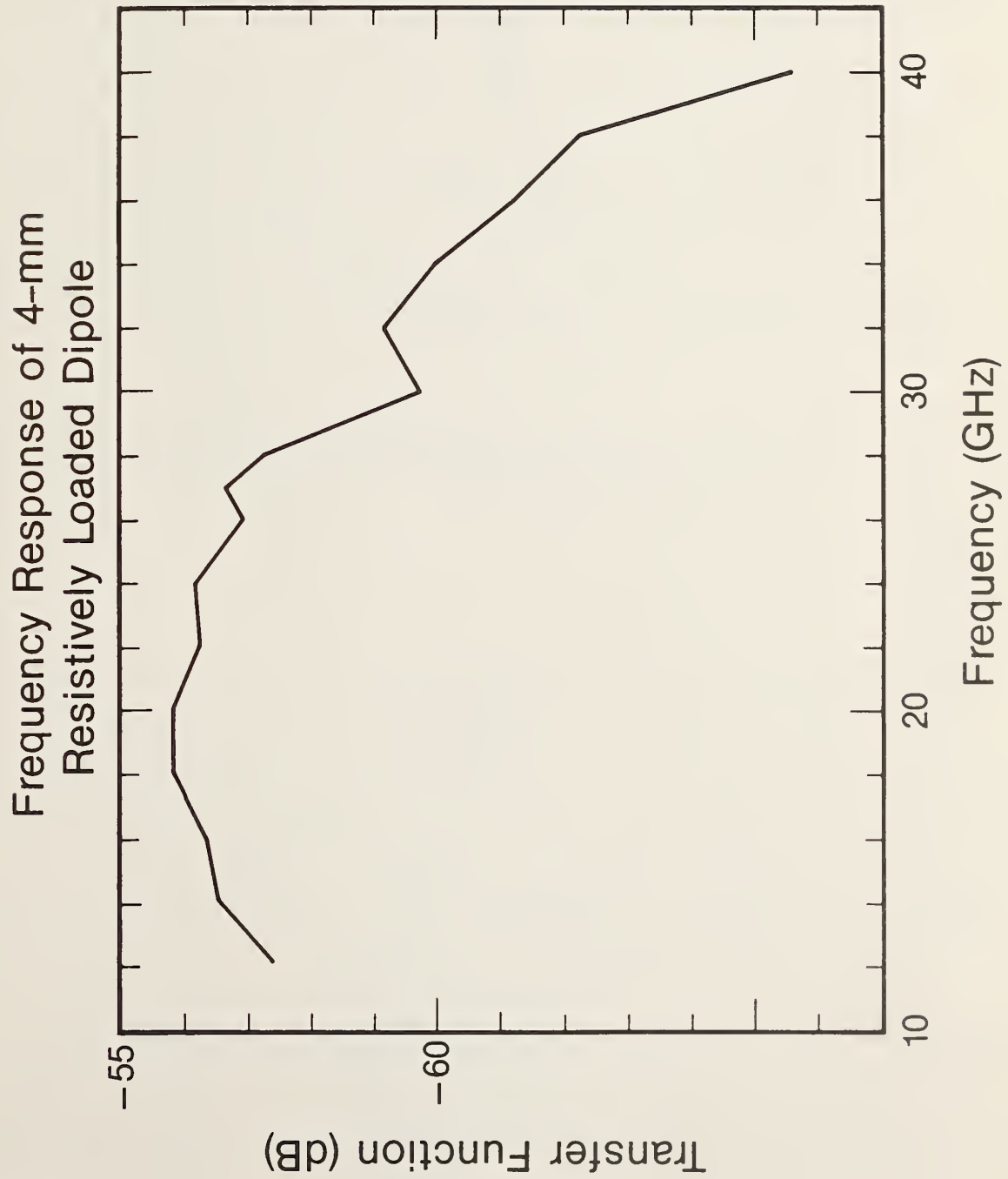


Figure 2 Frequency response of a 4-mm resistively loaded dipole.

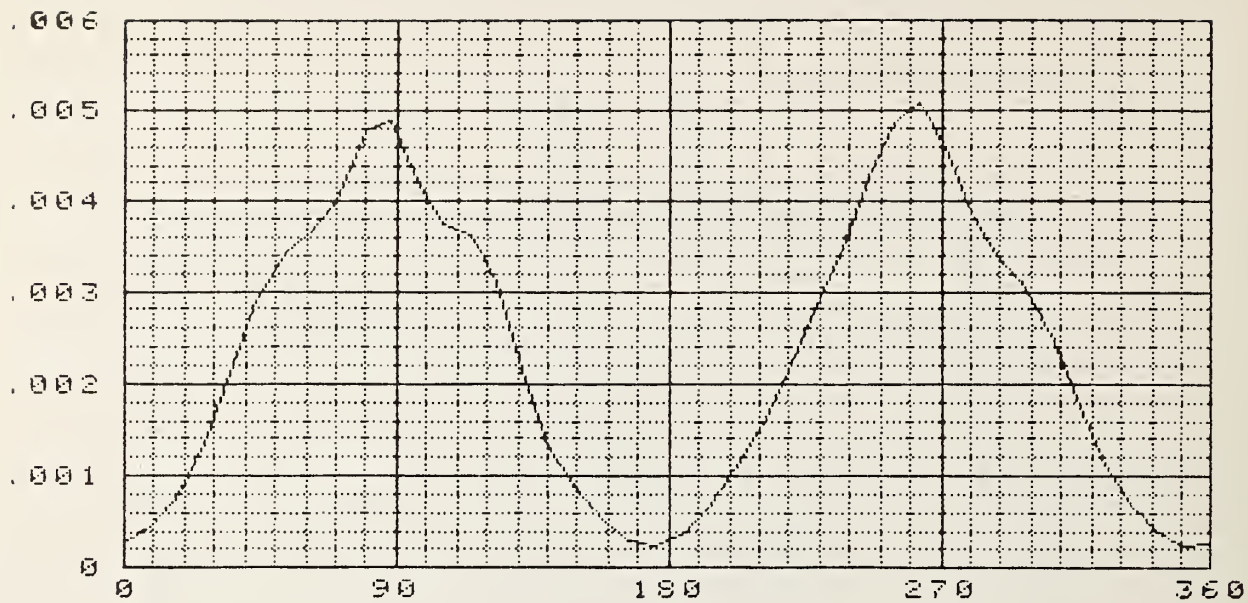


Figure 3a) Angular pattern of 4-mm resistively loaded dipole at 20 GHz. The abscissa is the angle between dipole axis and direction of the incident plane wave.

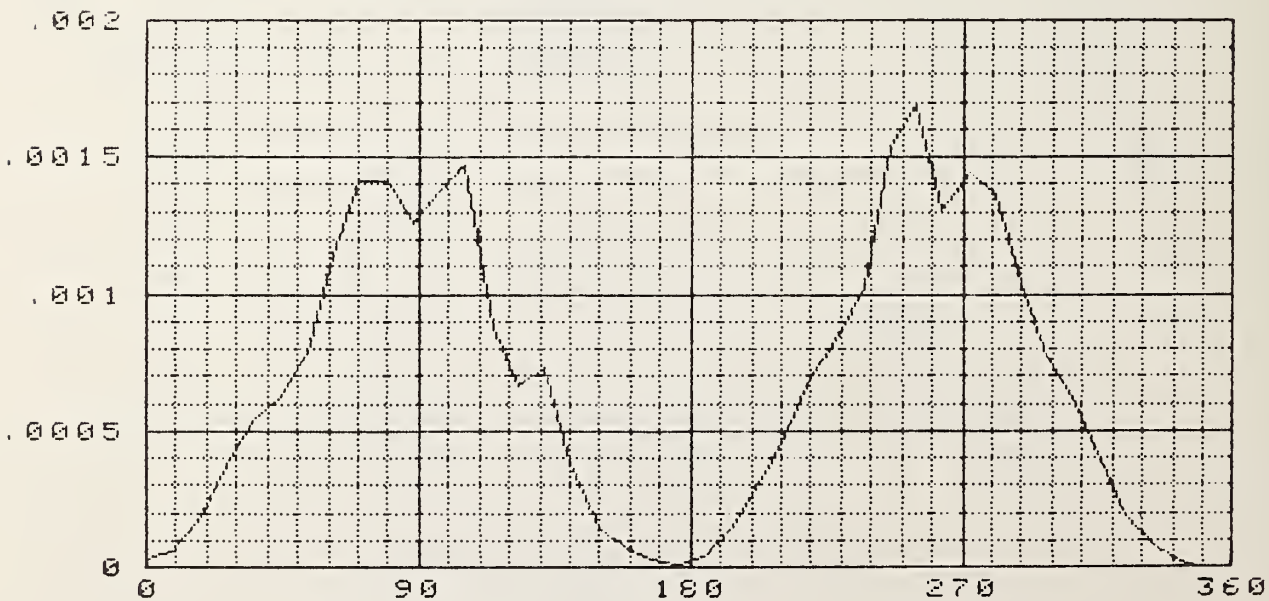


Figure 3b) Angular pattern at 30 GHz.

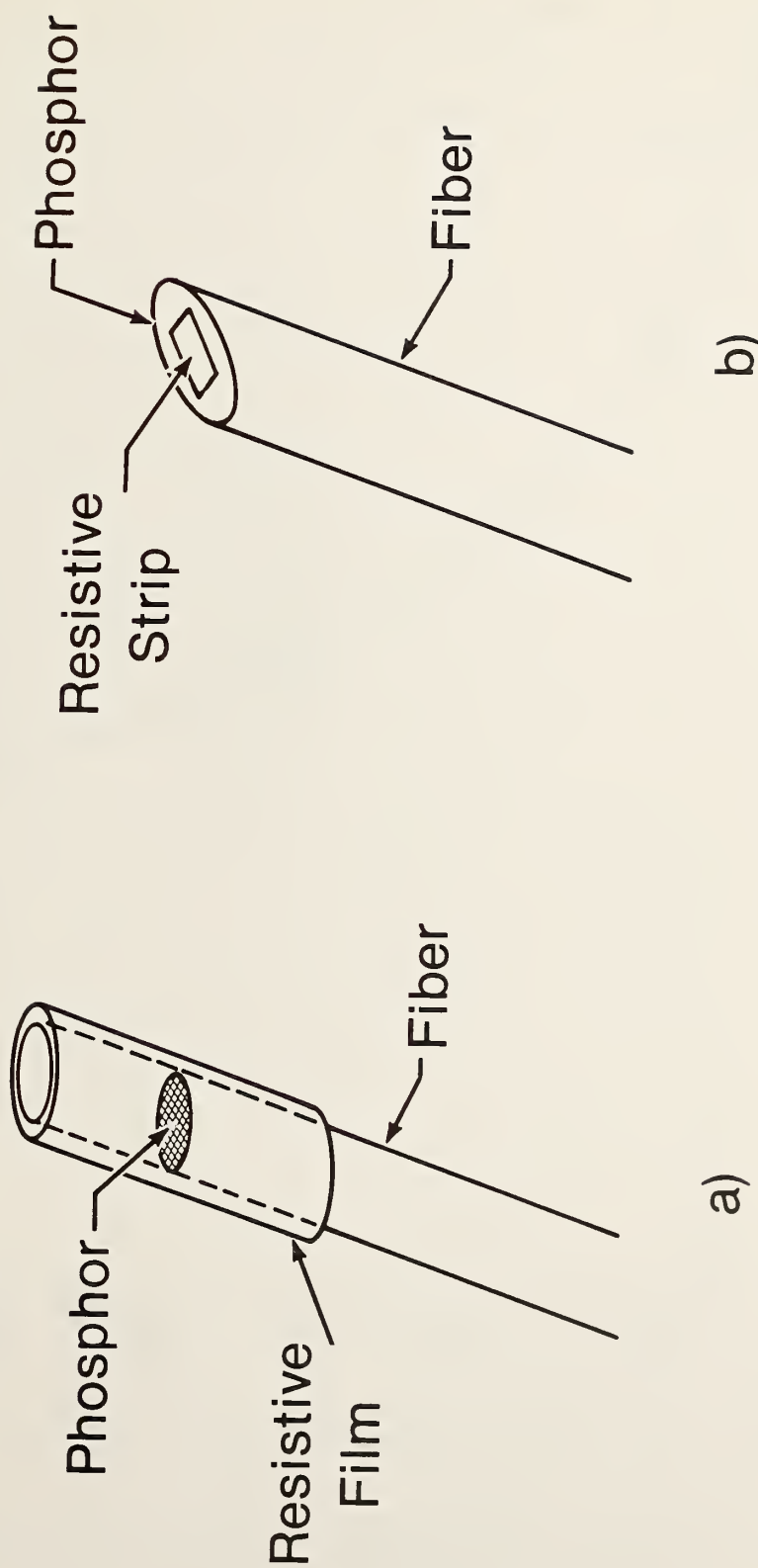


Figure 4 Two resistive-film configurations considered. a) Cylindrical coating. b) Resistive strip.

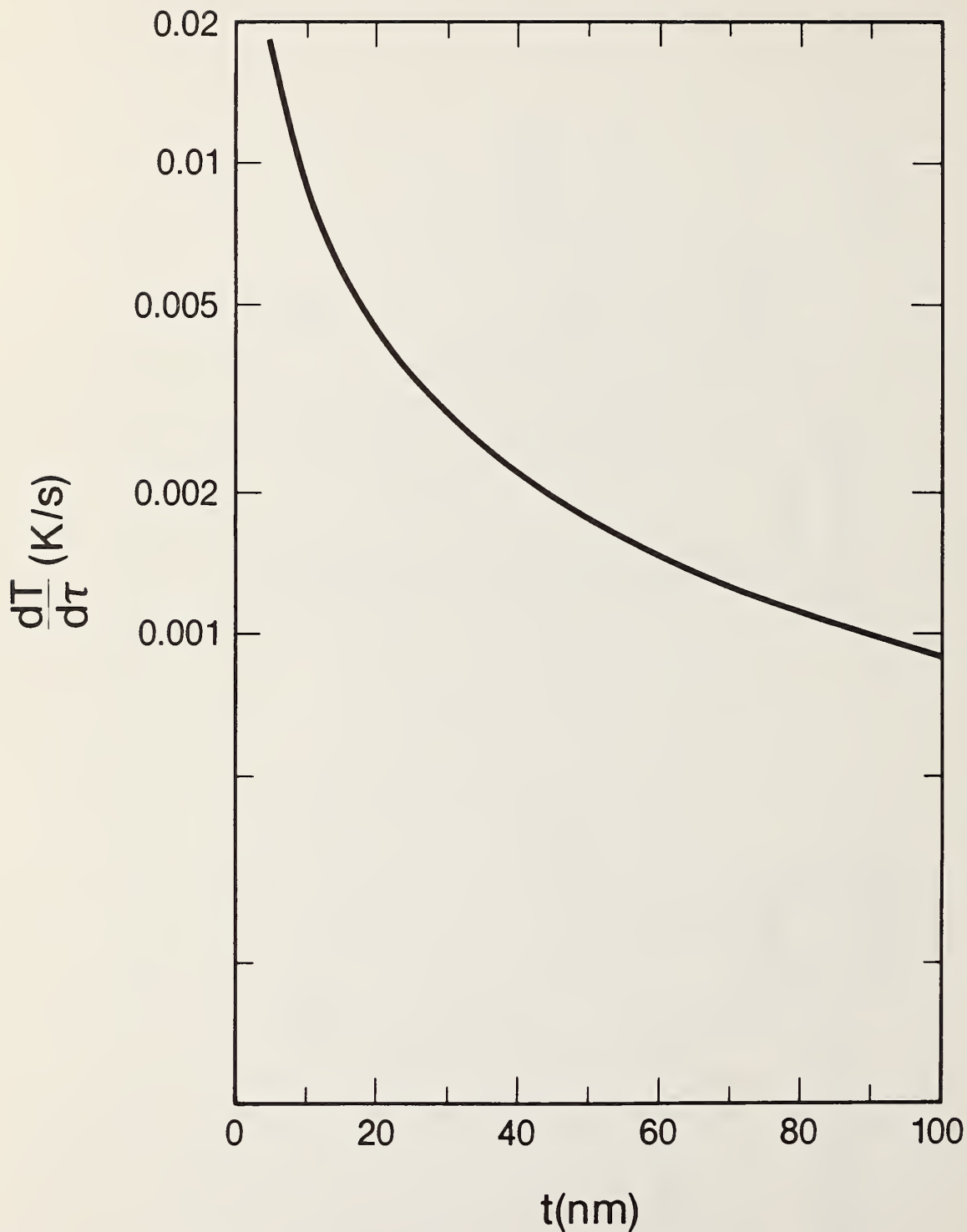


Figure 5 Calculated rate of temperature rise for resistive tubular cylinder in a 1-V/m 100-GHz field, as a function of cylinder thickness. The optimal conductivity was used for each thickness and the cylinder radius was 0.5 mm.

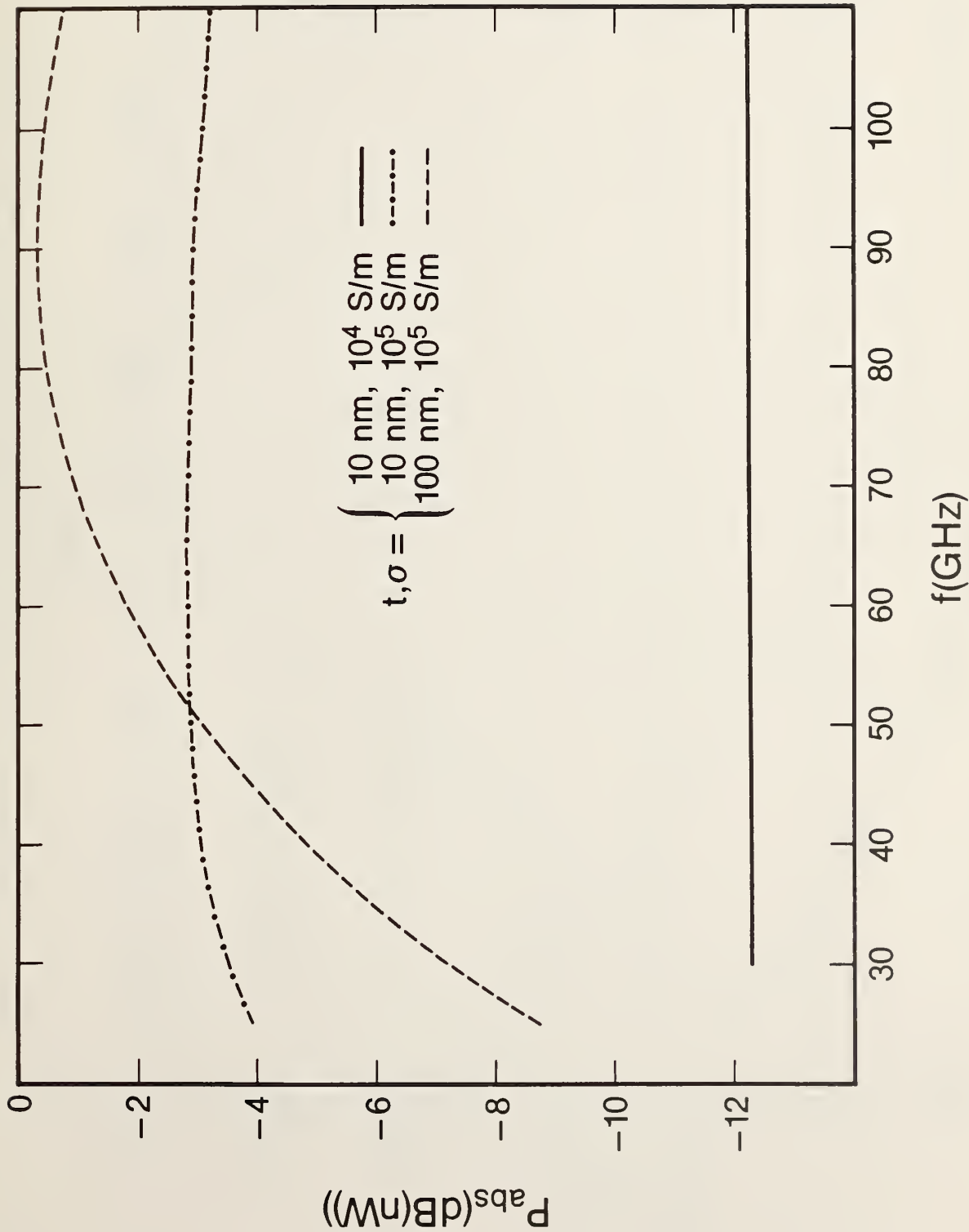


Figure 6 Calculated power absorbed by a tubular cylindrical dipole in a 1 V/m field as a function of frequency for three different choices of thickness and conductivity. The radius and full length in each case were 0.25 mm and 1.0 mm, respectively.

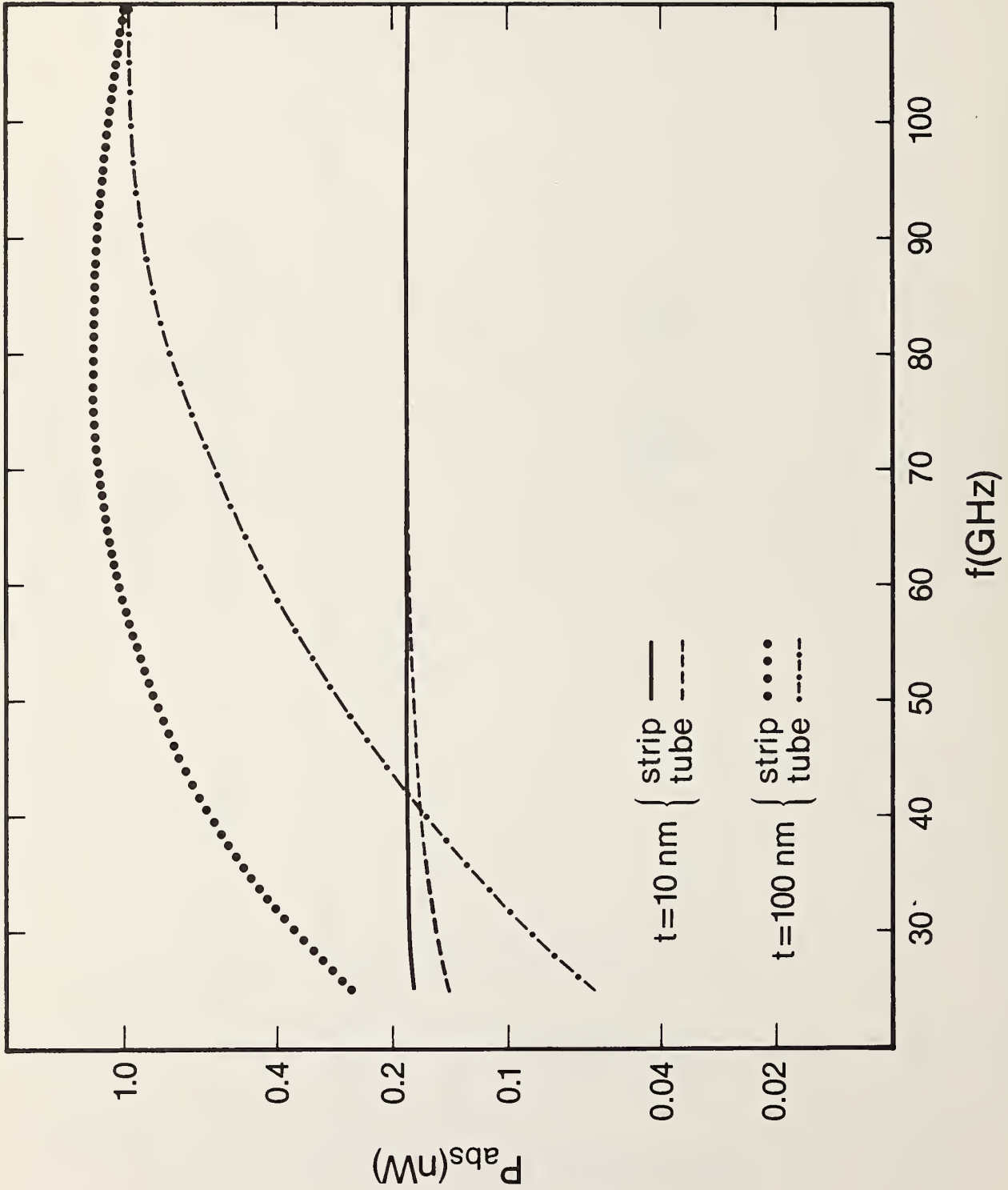


Figure 7 Comparison of the powers absorbed by a resistive tubular cylinder and a resistive strip of the same thickness and surface area.

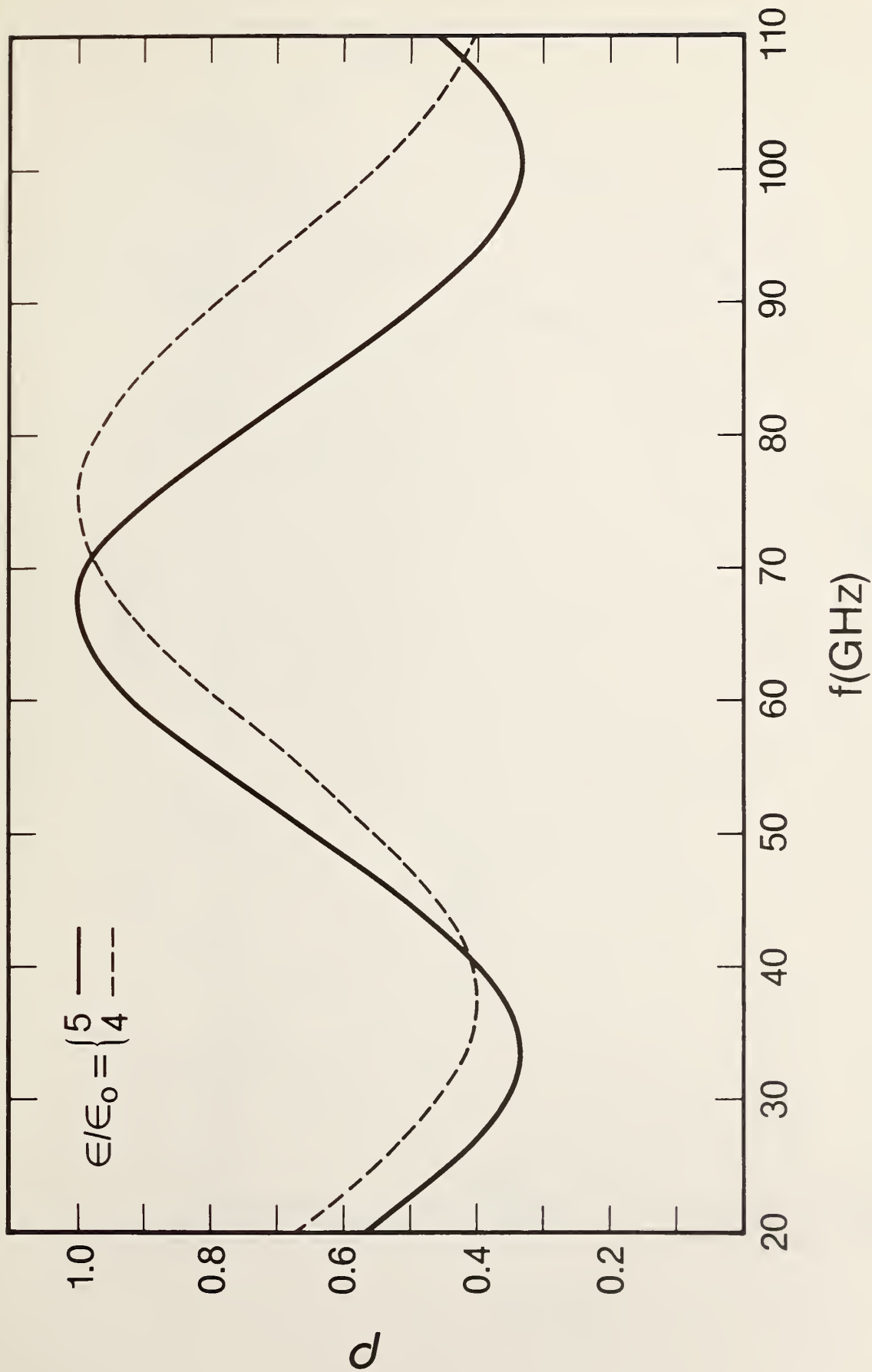


Figure 8a) Ratio of the total field to the incident field at the face of a dielectric slab as a function of frequency, assuming a normally incident plane wave. The slab is assumed to be 1 mm thick and have very large transverse extent.

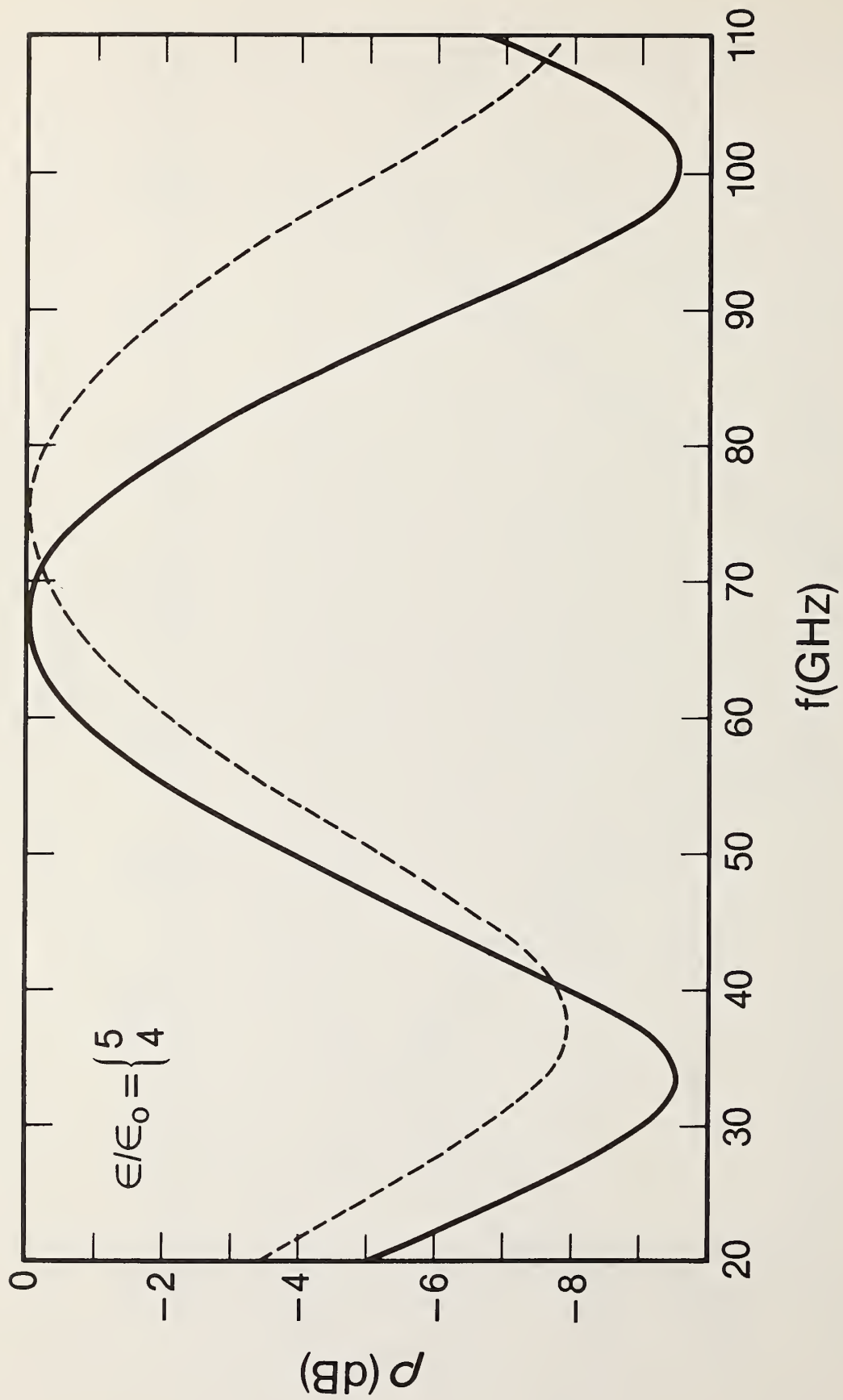
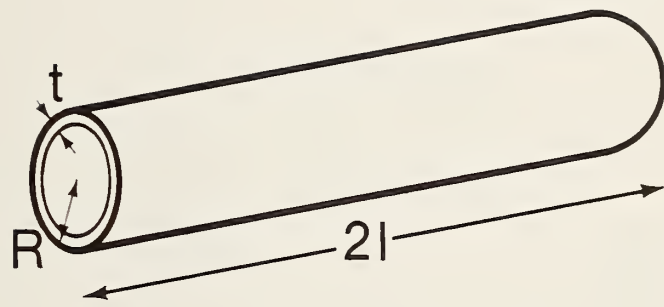
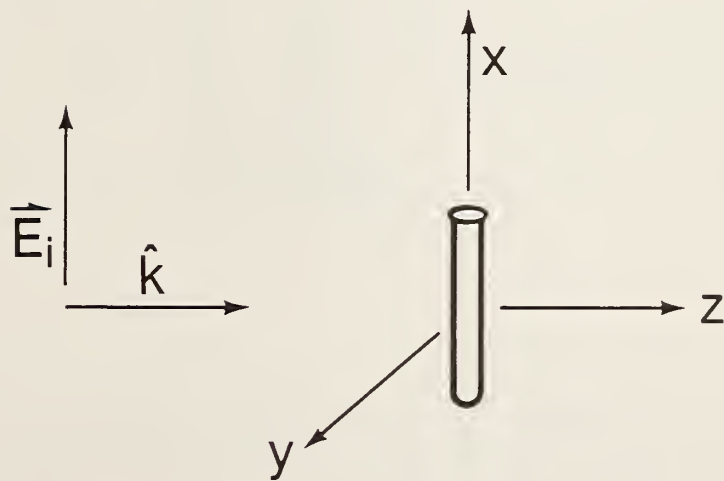


Figure 8b) As in figure 8a), in dB.



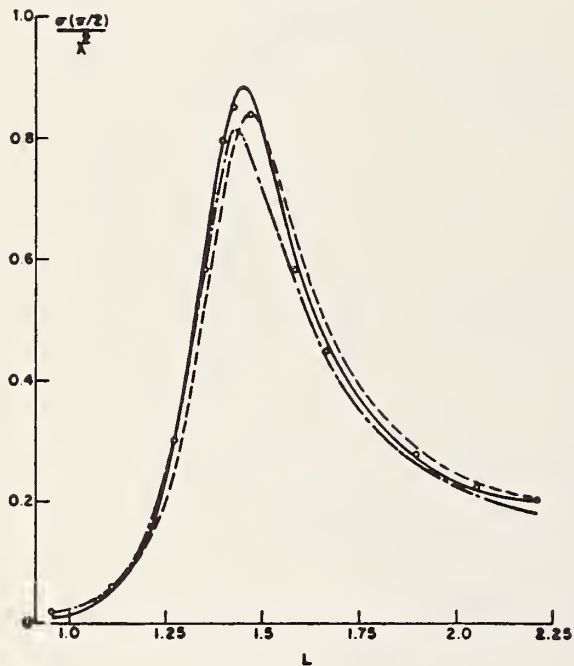
(a)

Figure 9a) Dimensions of resistive tubular cylinder.

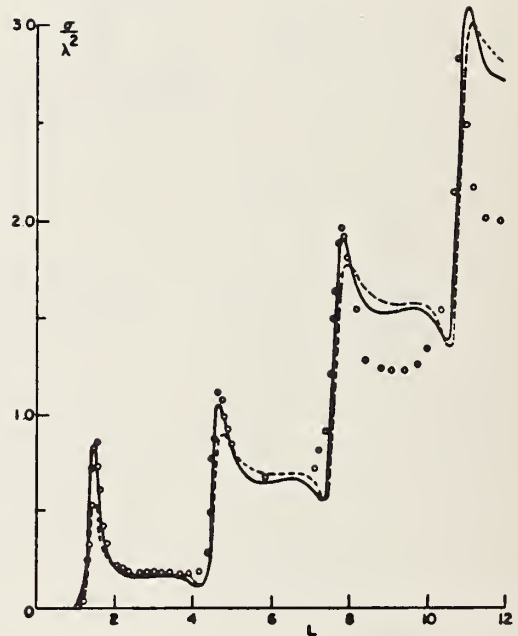


(b)

Figure 9b) Geometry for scattering from cylinder.



(a)



(b)

Figure 10 RCS of a single perfectly conducting wire as a function of  $L = 2\pi\ell/\lambda$ . Curves represent different calculations; circles are measurement results. Taken from [27].

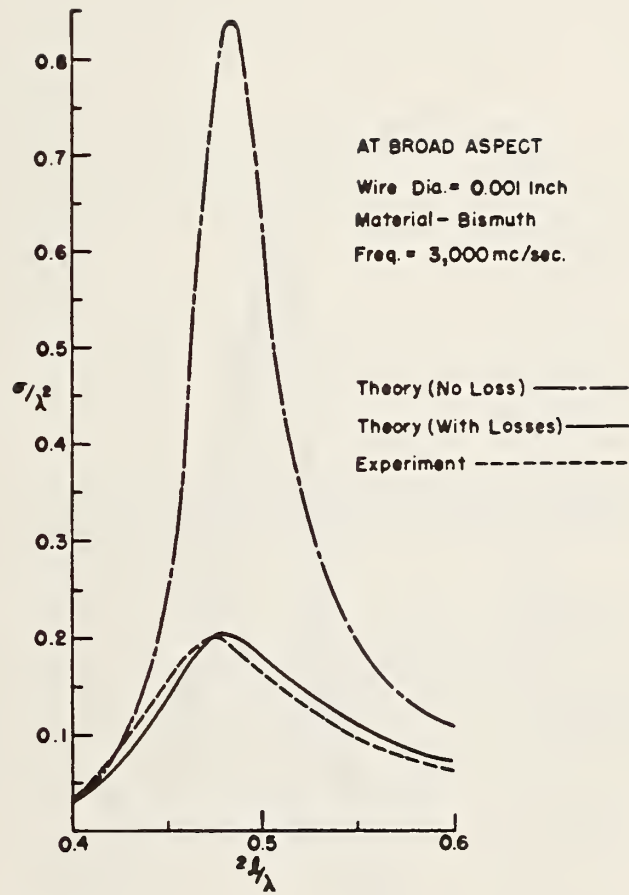


Figure 11 Calculated and measured RCS for a lossy wire. Taken from [28].

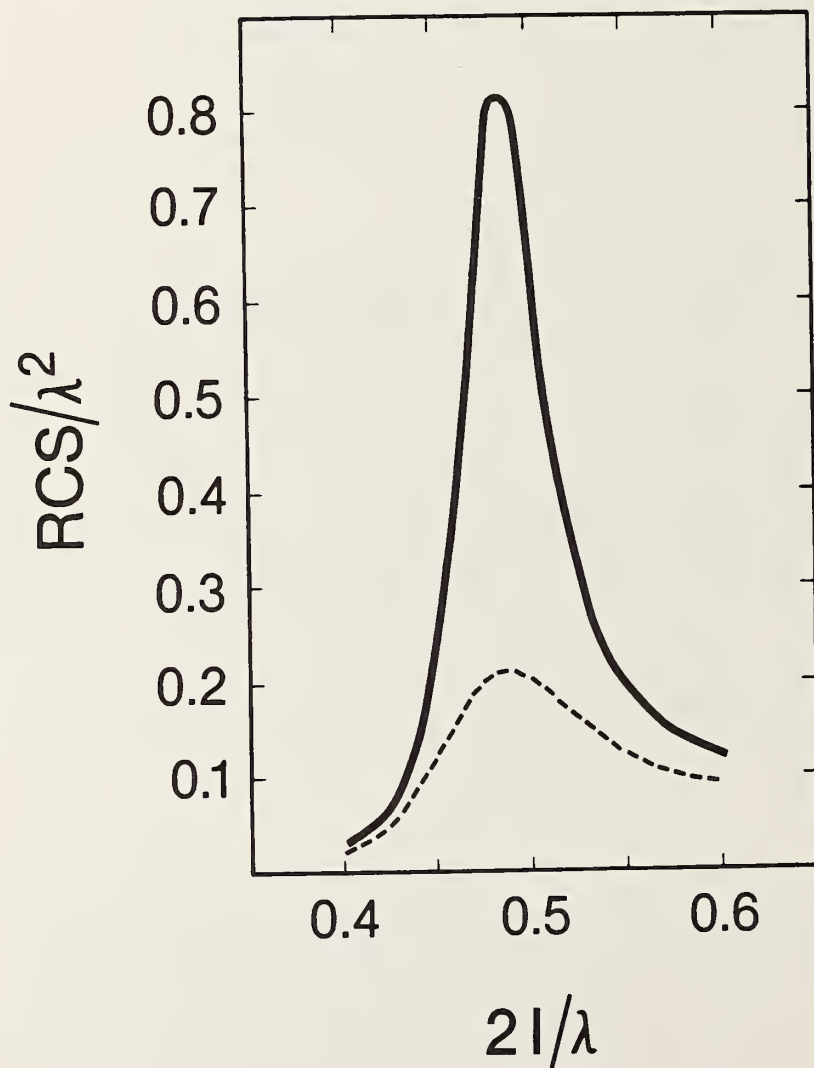


Figure 12 RCS for lossless (continuous curve) and lossy (dashed curve) wire, computed using SAM.

U.S. DEPT. OF COMM. <b>BIBLIOGRAPHIC DATA SHEET</b> <i>(See instructions)</i>	<b>1. PUBLICATION OR REPORT NO.</b> NBSIR 88-3084	<b>2. Performing Organ. Report No.</b>	<b>3. Publication Date</b> February 1988
<b>4. TITLE AND SUBTITLE</b> POSSIBLE DESIGNS FOR ELECTRIC-FIELD-STRENGTH PROBES FOR MILLIMETER WAVES			
<b>5. AUTHOR(S)</b> J. Randa, M. Kanda, and D. Melquist			
<b>6. PERFORMING ORGANIZATION</b> <i>(If joint or other than NBS, see instructions)</i> NATIONAL BUREAU OF STANDARDS DEPARTMENT OF COMMERCE WASHINGTON, D.C. 20234		<b>7. Contract/Grant No.</b>	<b>8. Type of Report &amp; Period Covered</b>
<b>9. SPONSORING ORGANIZATION NAME AND COMPLETE ADDRESS</b> <i>(Street, City, State, ZIP)</i> Naval Ocean Systems Center San Diego, CA 92152-5122			
<b>10. SUPPLEMENTARY NOTES</b>  <input type="checkbox"/> Document describes a computer program; SF-185, FIPS Software Summary, is attached.			
<b>11. ABSTRACT</b> <i>(A 200-word or less factual summary of most significant information. If document includes a significant bibliography or literature survey, mention it here)</i>  Various designs are considered for electric-field probes for the frequency range 26-110 GHz. Two particular designs are investigated in some detail. A resistively tapered dipole antenna with a diode detector shows promise for frequencies up to about 40 GHz. The second design is based on a fiber-optically sensed temperature sensor to detect the heating of a resistive strip. If its sensitivity can be increased significantly, this design may be capable of operating to frequencies above 100 GHz.			
<b>12. KEY WORDS</b> <i>(Six to twelve entries; alphabetical order; capitalize only proper names; and separate key words by semicolons)</i> electric-field probe; flouroptic temperature sensor; millimeter waves; resistively tapered dipole.			
<b>13. AVAILABILITY</b> <input checked="" type="checkbox"/> Unlimited <input type="checkbox"/> For Official Distribution. Do Not Release to NTIS <input type="checkbox"/> Order From Superintendent of Documents, U.S. Government Printing Office, Washington, D.C. 20402. <input checked="" type="checkbox"/> Order From National Technical Information Service (NTIS), Springfield, VA. 22161		<b>14. NO. OF PRINTED PAGES</b> 40	<b>15. Price</b>





